

Homeostatic adaptation to endoplasmic reticulum stress depends on Ire1 kinase activity

Claudia Rubio,^{1,2} David Pincus,^{1,2} Alexei Korenykh,^{1,2} Sebastian Schuck,^{1,2} Hana El-Samad,² and Peter Walter^{1,2}

¹Howard Hughes Medical Institute and ²Department of Biochemistry and Biophysics, University of California, San Francisco, San Francisco, CA 94158

Accumulation of misfolded proteins in the lumen of the endoplasmic reticulum (ER) activates the unfolded protein response (UPR). Ire1, an ER-resident transmembrane kinase/RNase, senses the protein folding status inside the ER. When activated, Ire1 oligomerizes and trans-autophosphorylates, activating its RNase and initiating a nonconventional mRNA splicing reaction. Splicing results in production of the transcription factor Hac1 that induces UPR target genes; expression of these genes restores ER homeostasis by increasing its protein folding capacity and allows abatement of UPR signaling.

Here, we uncouple Ire1's RNase from its kinase activity and find that cells expressing kinase-inactive Ire1 can regulate Ire1's RNase, splice *HAC1* mRNA, produce Hac1 protein, and induce UPR target genes. Unlike wild-type *IRE1*, kinase-inactive Ire1 cells display defects in Ire1 deactivation. Failure to properly inactivate Ire1 causes chronic ER stress and reduces cell survival under UPR-inducing conditions. Thus, Ire1-catalyzed phosphoryl-transfer aids disassembly of Ire1 signaling complexes and is a critical component of the UPR homeostatic feedback loop.

Introduction

In eukaryotic cells, all proteins that enter the secretory pathway must pass through the ER to be properly folded and modified. When the demand for protein folding in the ER exceeds the capacity of the compartment, misfolded proteins accumulate and activate the unfolded protein response (UPR). Activation of the UPR induces a broad transcriptional program, resulting in increased production of ER-resident protein folding machinery and ER-associated degradation components (Travers et al., 2000), and leading to ER expansion (Bernales et al., 2006; Schuck et al., 2009). As a consequence, the protein folding capacity of the ER is increased and protein folding stress is relieved. The UPR thus serves as a homeostatic feedback loop that monitors the state of the ER and alters gene expression to adjust protein folding capacity according to need, thereby restoring proper function to the ER.

In the yeast *Saccharomyces cerevisiae*, the UPR is initiated by an ER-resident transmembrane sensor, Ire1 (Cox et al., 1993; Mori et al., 1993). When activated by the accumulation of misfolded proteins, Ire1 removes a 252-nucleotide inhibitory intron from the mRNA encoding Hac1, a bZIP transcription

factor that up-regulates transcription of UPR target genes (Cox and Walter 1996; Mori et al., 1996; Travers et al., 2000). Removal of this intron and ligation of the severed exons by tRNA ligase produces a spliced form of *HAC1* mRNA that is efficiently translated into the Hac1 transcription factor (Cox and Walter 1996; Rügsegger et al., 2001). Because unspliced *HAC1* mRNA is not translated before the excision of this intron, Ire1 RNase activation provides the key switch in UPR signaling.

Ire1 is a single-pass transmembrane protein with one domain in the ER lumen and two domains, a kinase and an RNase, in the cytosol (Cox et al., 1993; Sidrauski and Walter 1997). The luminal domain of Ire1 senses unfolded proteins and, once activated, drives Ire1 oligomerization (Shamu and Walter 1996; Credle et al., 2005). Ire1's luminal domain resembles the peptide-binding domain of antigen-presenting major histocompatibility complexes. We have proposed that direct binding of unfolded polypeptide chains to a presumed peptide binding groove in this domain provides the activating signal (Credle et al., 2005; Pincus et al., 2010), although more indirect models of Ire1 activation have also been proposed (Bertolotti et al., 2000; Okamura et al., 2000; Kimata et al., 2004). Lateral oligomerization

C. Rubio and D. Pincus contributed equally to this paper.

Correspondence to Peter Walter: peter@walterlab.ucsf.edu

Abbreviations used in this paper: HPL, hyper-phosphorylated loop; SR, splicing reporter; UPR, unfolded protein response; UTR, untranslated region; WT, wild type.

© 2011 Rubio et al. This article is distributed under the terms of an Attribution-Noncommercial-Share Alike-No Mirror Sites license for the first six months after the publication date [see <http://www.rupress.org/terms>]. After six months it is available under a Creative Commons License [Attribution-Noncommercial-Share Alike 3.0 Unported license, as described at <http://creativecommons.org/licenses/by-nc-sa/3.0/>].

Supplemental Material can be found at:
<http://jcb.rupress.org/content/suppl/2011/03/25/jcb.201007077.DC1.html>
Original image data can be found at:
<http://jcb-dataviewer.rupress.org/jcb/browse/4056>

brings the cytosolic portion of neighboring Ire1 molecules into proximity, which promotes trans-autophosphorylation of Ire1 kinase and activation of the RNase (Shamu and Walter 1996).

Mutation of essential catalytic residues and phosphorylation sites in the Ire1 kinase domain block *HAC1* mRNA splicing and prevent up-regulation of UPR target genes (Cox et al., 1993; Mori et al., 1993; Shamu and Walter 1996), suggesting that phosphorylation by Ire1 kinase during activation is essential for RNase function. However, if the nucleotide-binding pocket of Ire1 kinase is mutated to specifically accommodate the ATP-competitive drug 1NM-PP1, Ire1 retains RNase activity in response to ER stress, showing that the requirement for phosphorylation can be entirely bypassed (Papa et al., 2003). Occupation of the engineered 1NM-PP1 binding pocket is sufficient to cause the conformational change in Ire1 that activates the RNase. Because phosphorylation sites are necessary for RNase function but phosphorylation by itself appears dispensable, the functional significance of phosphoryl-transfer by Ire1 kinase has remained unclear.

Evidence from studies of Ire1-like enzymes supports the idea that phosphoryl-transfer mediated by the kinase is indeed dispensable for nuclease activation. RNase L, a close homologue of Ire1, is a cytosolic, ligand-activatable RNase that has lost kinase activity but retained a catalytically inactive pseudokinase domain (Dong et al., 2001). In contrast, the kinase activity of Ire1 has been preserved in evolution, suggesting a functional role for Ire1-mediated phosphoryl-transfer. Although previous findings with 1NM-PP1-sensitized Ire1 kinase are in apparent contradiction with this idea, those data show only that Ire1 kinase activity can be bypassed without consequence for RNase activation; they do not rule out a possible role for the kinase in the broader scope of UPR biology.

In this study, we explored the role of the Ire1 kinase function in vitro and in vivo by rationally designed, conservative mutagenesis of central catalytic residues in the Ire1 kinase-active site. Mutations were designed to preserve interactions between ATP cofactor and Ire1 but to selectively disrupt catalytic phosphoryl-transfer. We show that these mutations yield a kinase-inactive Ire1 that retains wild-type (WT) RNase activity in living cells. This variant of Ire1 is activated by unfolded protein accumulation without a requirement for exogenous drugs, such as 1NM-PP1, thereby eliminating potential complications of off-target effects of the drug within the cell. These studies confirmed the view that Ire1's kinase domain regulates its RNase activity, but also revealed a critical role for phosphoryl-transfer in the homeostatic feedback of the UPR.

Results

Mutations in Ire1 kinase abolish phosphoryl-transfer but preserve RNase activity

Based on sequence conservation between Ire1 and related CDK2-like kinases as well as the recently solved crystal structures of the cytosolic portion of Ire1 (Lee et al., 2008; Korennykh et al., 2009), we designed an Ire1 variant with uncoupled kinase and RNase activities. To this end, we identified two catalytic

residues, D797 and K799, in the nucleotide-binding pocket of Ire1 kinase. These residues are predicted to coordinate the terminal phosphate of ATP bound to Ire1 kinase (Fig. 1 A), and, by analogy to other kinases, are required to catalyze phosphotransfer (Lee et al., 2008). We reasoned that mutating these residues to asparagines would preserve overall steric packing, hydrophobicity, and hydrogen bonding at the kinase-active site but disable proton transfer and thereby abolish phosphorylation (Fig. S1 A). Thus, we expected that the mutant Ire1(D797N,K799N) would be kinase inactive but still able to activate its RNase via nucleotide binding.

To carry out in vitro studies, we recombinantly expressed and purified the cytosolic portion of Ire1 WT and mutant Ire1. These constructs consisted of kinase and RNase domains preceded at the N terminus by 32 amino acids derived from the linker region that tethers the kinase domain to the transmembrane region. We previously showed that this peptide extension is important, as it enhances Ire1's ability to activate its RNase by up to four orders of magnitude (Korennykh et al., 2009). We term these constructs Ire1KR32 (WT) (Korennykh et al., 2009) and Ire1KR32(D797N,K799N).

MALDI mass spectrometry analyses have shown that WT Ire1KR32 is highly phosphorylated when purified from *Escherichia coli*, likely as a result of autophosphorylation (Korennykh et al., 2009). Phosphorylation is evident in the mass-to-charge ratio (*M/z*) of WT Ire1KR32, which is higher than expected based on its theoretical molecular weight (Fig. S1 B). The shift of ~1.3 kD is consistent with the presence of ~17 phosphates and can be ameliorated by phosphatase treatment (Fig. S1 C). In contrast, purified Ire1KR32(D797N,K799N) has an *M/z* value that is precisely as expected based on its primary sequence, indicating that this protein is entirely unphosphorylated (Fig. S1 B; and see Fig. S7 in Korennykh et al., 2009). These data suggest that Ire1KR32(D797N,K799N) is kinase inactive.

To confirm that Ire1KR32(D797N,K799N) was indeed kinase inactive, we measured trans-autophosphorylation of the recombinant proteins in an in vitro kinase assay. As expected, WT Ire1KR32 showed robust trans-autophosphorylation (Fig. 1 B, lanes 1–3) whereas Ire1KR32(D797N,K799N) exhibited no detectable kinase activity (Fig. 1 B, lanes 4–6). To show that the kinase-inactive Ire1 mutant is properly folded and is a competent substrate for phosphorylation, we mixed recombinant kinase-inactive Ire1 protein with a shorter WT version, Ire1KR, lacking the 32-amino acid peptide extension (Korennykh et al., 2009). This enzyme retains WT kinase activity (Fig. 1 B, lanes 7–9) and can be distinguished from the Ire1KR32 versions by its lower molecular weight. When we mixed Ire1KR in vitro with Ire1KR32(D797N,K799N), we detected robust phosphorylation of the mutant enzyme (Fig. 1 B, lanes 10–12; top bands). In these mixing reactions, the top bands corresponding to the kinase-inactive variant of Ire1 were more extensively labeled with radioactive phosphate than WT enzyme. This is likely due to the greater number of unphosphorylated residues in kinase-inactive Ire1 available for phosphorylation when introduced to kinase-active enzyme.

Based on the previous observation that occupation of the active site of Ire1 kinase by nucleotide cofactor is sufficient

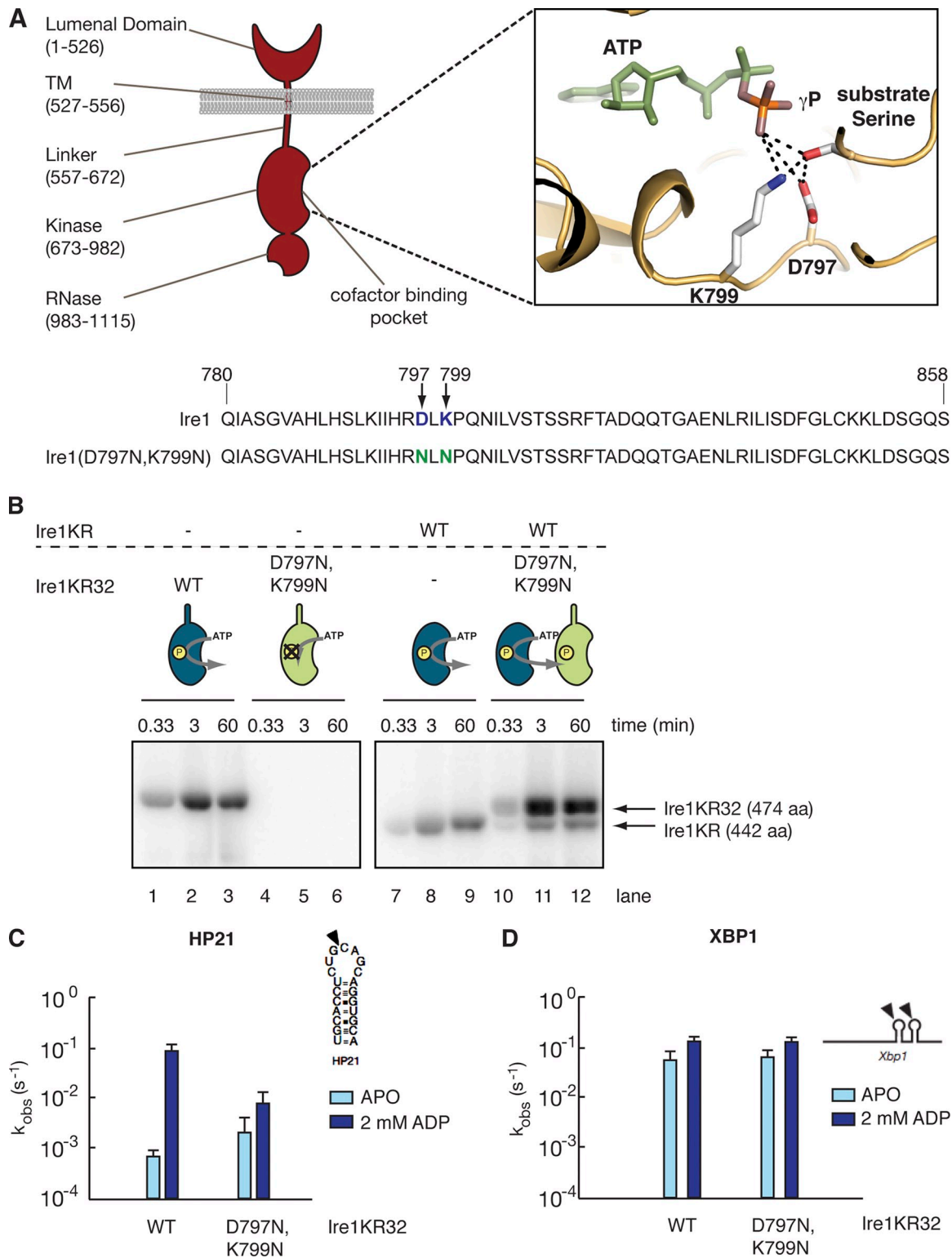


Figure 1. Mutations in Ire1 kinase abolish phosphate transfer but preserve RNase activity. (A) A schematic representation of Ire1 depicting the location of each functional domain. Residues D797 and K799 in the nucleotide-binding pocket of the kinase domain hydrogen bond with the terminal phosphate of ATP to catalyze phosphate transfer to the substrate serine. Mutation of D797 and K799 to noncatalytic asparagines is predicted to block phosphate transfer but allow for ATP binding. (B) The kinase activity of recombinant Ire1KR32 (WT, 474 amino acids; lanes 1–3) and Ire1KR32(D797N,K799N) (lanes 4–6) were measured in an in vitro kinase assay. Recombinant Ire1 was mixed with $0.033 \mu\text{M}$ $[\gamma^{32}\text{P}]\text{-ATP}$ and incubated at 30°C for the time indicated. Reactions were stopped in 1% SDS loading buffer and separated by SDS-PAGE. A truncated version of WT Ire1, Ire1KR (442 amino acids; lanes 7–9), was mixed with Ire1KR32(D797N,K799N) (lanes 10–12). (C and D) In vitro RNA cleavage assays were performed using purified substrate RNA, HP21 (C) or *Xbp1* (D), and either WT Ire1KR32 or Ire1KR32(D797N,K799N). Reactions were performed in the presence and absence of 2 mM ADP. The lower sensitivity of the *Xbp1* mRNA cleavage reaction to the ADP cofactor during cleavage suggests that a longer RNA substrate may independently stabilize the Ire1 oligomer, perhaps by bridging between multiple adjacent monomers. Bar values were obtained from single-exponential fitting of time courses. Error bars show standard errors of the single-exponential fitting. The time courses were repeated multiple times and k_{obs} values reproduced within twofold.

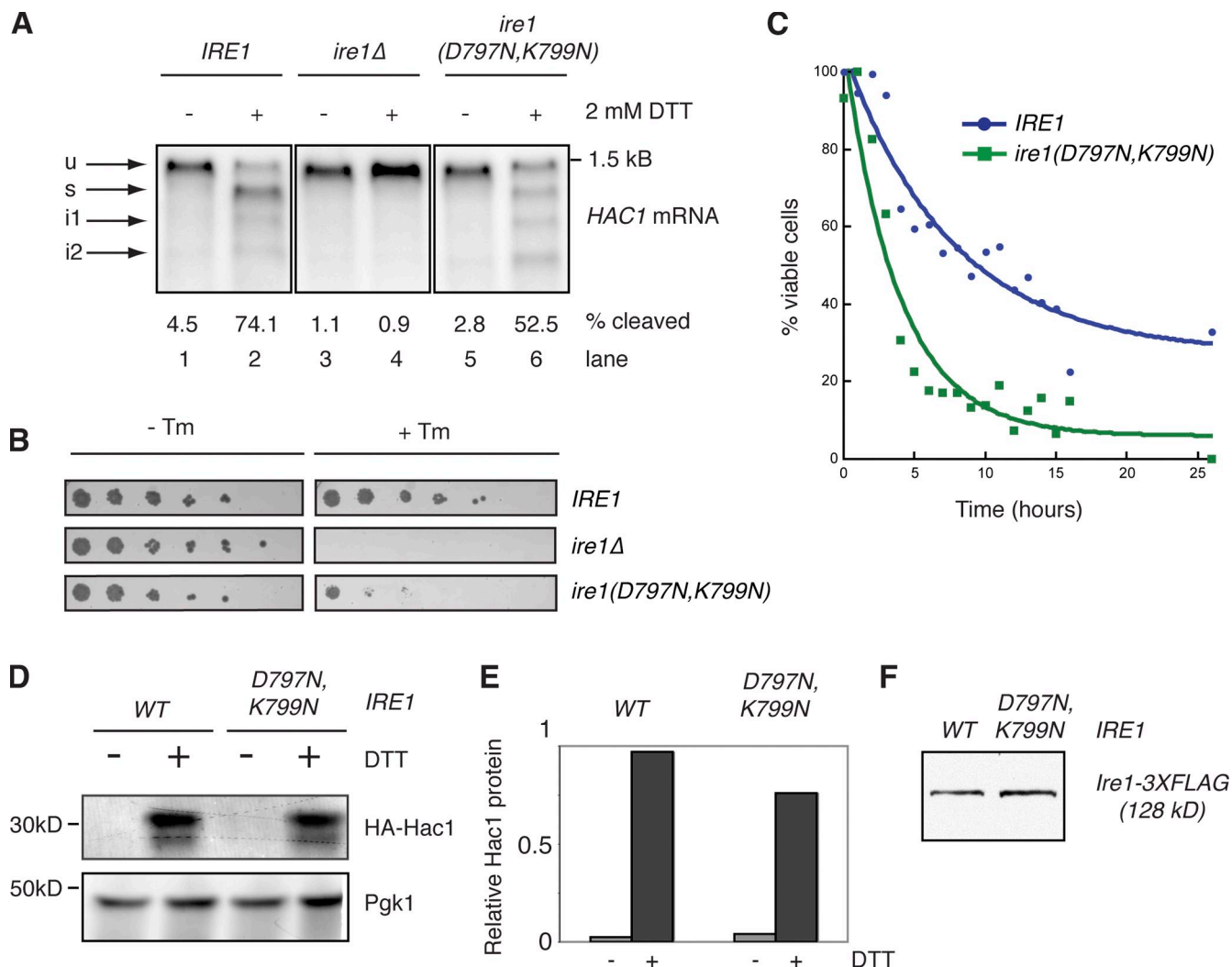


Figure 2. Ire1 kinase activity, uncoupled from HAC1 mRNA splicing, is important for cell survival during the UPR. (A) Cells bearing WT *IRE1* (lanes 1 and 2), a deletion of *ire1* (lanes 3 and 4), or *ire1*(D797N,K799N) (lanes 5 and 6) were left uninduced (–) or induced with 2 mM DTT (+). *HAC1* mRNA splicing was analyzed by Northern blotting. The positions of the unspliced (u; 1449 nucleotides) and spliced (s; 1197 nucleotides) forms of *HAC1* mRNA are indicated with arrows. Splicing intermediate i1 (980 nucleotides) corresponds to the 5' exon–intron hybrid species, whereas i2 (728 nucleotides) corresponds to the 5' exon alone. (B) Cells carrying WT *IRE1*, a deletion of *ire1*, or *ire1*(D797N,K799N) were grown in culture, diluted to equal cell number, serially diluted 1:5, and plated onto permissive medium (–Tm) or medium containing 0.25 μg/ml tunicamycin (+Tm). (C) WT *IRE1* or *ire1*(D797N,K799N) cells were grown in culture to OD₆₀₀ 0.2, the UPR was induced by the addition of 2 mM DTT. The value for percent viable cells was determined by measuring the number of colony-forming units over time (see Materials and methods). DTT was refreshed and cells were kept at an OD at or below 0.2 throughout the duration of the experiment. (D) WT or mutant *ire1* cells carrying HA-tagged Hac1 were left uninduced or induced with 2 mM DTT, and total protein was isolated. Samples were separated by SDS-PAGE and subjected to Western blotting using an anti-HA antibody or an anti-PGK1 antibody. (E) Hac1 protein was quantified, normalized to PGK1 levels, and plotted. (F) Total protein was isolated from WT- or *Ire1*(D797N,K799N)-expressing cells, separated by SDS-PAGE, and subjected to Western blotting using an anti-FLAG antibody. *Ire1* protein levels are equivalent in WT and *ire1*(D797N,K799N) cells.

to cause activation of the RNase, we expected that *Ire1*KR32(D797N,K799N) would retain RNase activity and that its activity would be stimulated by the presence of nucleotide. To test this prediction, we measured RNase activity in an *in vitro* cleavage assay using HP21, a previously characterized small substrate RNA containing a specific *Ire1* cleavage site, in the presence or absence of ADP cofactor. In previous experiments, ADP stimulated *Ire1*KR32's RNase activity by ~200-fold (Korennykh et al., 2009). Here, in the absence of cofactor, both enzymes exhibited the same basal RNase activity as *Ire1*KR32 (Fig. 1 C, “APO”), consistent with previous observations (Korennykh et al., 2009). Addition of ADP increased the RNase of *Ire1*KR32(D797N,K799N) 10-fold (versus ~100-fold

for WT *Ire1*KR32; Fig. 1 C, “ADP”). These data are consistent with the idea that binding of cofactor stimulates the RNase activity of *Ire1* in the absence of phosphorylation (Papa et al., 2003). In *in vitro* assays using the HP21 substrate, the RNase activity of *Ire1*KR32(D797N,K799N) was 10-fold lower than that of WT. However, when a larger 443-nt *Xbp1* mRNA-derived RNA fragment was used as a substrate (Korennykh et al., 2009), *Ire1*KR32(D797N,K799N) cleaved with a rate ($k_{\text{obs}} = 0.19 \text{ s}^{-1}$) indistinguishable from that of WT *Ire1*KR32 ($k_{\text{obs}} = 0.19 \text{ s}^{-1}$; Fig. 1 D). The *Xbp1* mRNA is a 400-nt substrate derived from the mammalian counterpart to *HAC1* mRNA. This substrate is cleaved by *Ire1* *in vitro* with kinetics identical to that of *HAC1* mRNA substrates of comparable length (unpublished data).

The low ADP sensitivity of the *Xbp1* mRNA cleavage reaction suggests a diminished requirement for cofactor during cleavage of this substrate. Present work in our laboratory is aimed at understanding the molecular mechanism of this phenomenon. This longer substrate RNA more closely resembles the endogenous *in vivo* substrate of Ire1 RNase, suggesting that kinase-inactive Ire1(D797N,K799N) should retain RNase function in living cells.

Ire1 kinase activity is dispensable for *HAC1* mRNA splicing but enhances cell survival under ER stress

Because our *in vitro* results showed that we had successfully uncoupled the kinase and RNase functions of Ire1, we used kinase-inactive Ire1(D797N,K799N) to directly investigate the role of Ire1 kinase activity *in vivo*. This approach afforded the first opportunity to ask this question without requiring the addition of exogenous drug as past studies necessitated.

Our *in vitro* studies predict that cells expressing Ire1(D797N,K799N) should splice *HAC1* mRNA upon UPR induction. To test this, we constructed a strain carrying a chromosomally integrated mutant *IRE1* allele as the sole copy of *IRE1* in the cell. We then induced the UPR and measured *HAC1* mRNA splicing by Northern blotting. We induced ER stress with DTT, which causes protein misfolding in the ER by disrupting disulfide bond formation. As predicted, spliced *HAC1* mRNA was produced upon DTT treatment in *ire1(D797N,K799N)* cells (Fig. 2 A, lanes 5 and 6). In contrast, *HAC1* mRNA was not spliced in *ire1Δ* cells (Fig. 2 A, lanes 3 and 4). In these experiments, *ire1(D797N,K799N)* proved mildly hypomorphic, as the amount of *HAC1* mRNA cleaved in the mutant cells was reduced compared with WT and *HAC1* splicing intermediates were more abundant at the time point taken. This was not due to differences in the expression levels of Ire1 (Fig. 2 F). Nevertheless, these data reinforce the notion that Ire1 kinase activity is not required for RNA splicing.

We were surprised to discover that splicing of *HAC1* mRNA in *ire1(D797N,K799N)* cells failed to ensure cell survival under ER stress. When plated on medium containing tunicamycin, a drug that induces the UPR by blocking glycosylation in the ER, *ire1(D797N,K799N)* cells displayed a severe growth defect (Fig. 2 B). This resulted from loss of cell viability rather than growth arrest: sustained ER stress killed *ire1(D797N,K799N)* cells significantly earlier than WT cells (Fig. 2 C).

In search of an explanation for this growth defect, we tested whether functional Hac1 protein was produced from spliced *HAC1* mRNA in *ire1(D797N,K799N)* cells. To this end, we measured Hac1 protein production and determined the scope of the transcriptional response by assessing global mRNA expression after UPR induction. WT *IRE1* or *ire1(D797N,K799N)* cells expressing HA-tagged Hac1 were treated with DTT to induce the UPR and probed for HA-Hac1 by Western blotting. *Ire1(D797N,K799N)* cells produced Hac1 protein at nearly WT levels (Fig. 2, D and E). Likewise, the microarray transcriptional profile of UPR-induced *ire1(D797N,K799N)* cells revealed a profile nearly indistinguishable from that of WT cells (Fig. S2 A). Canonical UPR target genes were up-regulated

with similar kinetics, and to a comparable extent, in WT and *ire1(D797N,K799N)* cells. Specific UPR target genes are highlighted in Fig. 3 A. Collectively, these data show that the observed reduction in *HAC1* mRNA splicing in *ire1(D797N,K799N)* cells does not lead to impairment of canonical UPR signaling.

One reason that a cell might die despite expression of target genes is that mRNAs are not translated. To confirm that protein products corresponding to UPR targets were also made, we determined Kar2 protein levels by Western blotting and measured global translation rates during the ER stress. The induction of Kar2 mirrored the microarray result for both WT and *ire1(D797N,K799N)* mutant cells (Fig. 3 B), confirming that expression of this canonical UPR target was intact in both strains. Furthermore, general translation rates were equivalent in both WT and *ire1(D797N,K799N)* cells (Fig. S2 B), indicating that global mRNA translation was not impaired in mutant cells. No explanation for the enhanced loss of cell viability of *ire1(D797N,K799N)* mutant cells was evident in these data.

As a consequence of UPR activation, the ER expands to meet the increased need for protein folding capacity (Cox et al., 1997; Bernales et al., 2006; Schuck et al., 2009). To further ensure that UPR signaling downstream of Ire1 was unimpaired, we measured ER expansion. Using a GFP-tagged version of the ER marker Sec63 (Prinz et al., 2000), we quantified expansion of the cortical ER before and after UPR induction in WT and *ire1(D797N,K799N)* cells. In confocal sections through the middle of unstressed cells, the cortical ER marked by Sec63-GFP is visible underneath the plasma membrane as a broken line because the tubular ER network appears in cross section. Upon ER stress, the cortical ER is converted into expanded membrane sheets and appears as a continuous line. Consistent with microarray data showing normal induction of target genes, UPR-mediated ER expansion occurred normally in mutant cells (Fig. 3, C and D). Thus, the slight reduction in Hac1 protein produced in *ire1(D797N,K799N)* cells (Fig. 2 E) did not weaken UPR events downstream of Hac1 protein production. Collectively, the data presented thus far indicate that canonical UPR activation remains intact in *ire1(D797N,K799N)* cells.

Ire1(D797N,K799N) fails to adapt to sustained ER stress

The homeostatic feedback response that is mediated by the UPR is characterized by an activation phase in which Ire1 begins to signal and an adaptive phase that occurs when cells adjust to ER stress and Ire1 is turned off (Pincus et al., 2010). Because our findings indicate that Ire1 activation and induction of its downstream transcriptional targets are normal in *ire1(D797N,K799N)* cells, we set out to examine the dynamics of Ire1 activation and attenuation in *ire1(D797N,K799N)* cells. To this end, we took advantage of a splicing reporter, termed SR, previously developed in our laboratory (Aragón et al., 2009). In the SR, the *HAC1* ORF has been replaced by that of *GFP* (Fig. 4 A), while the intron as well as the 5' and 3' untranslated regions (UTRs) of the *HAC1* mRNA are maintained so that translational inhibition of SR mimics that of the *HAC1* mRNA. Ire1-mediated splicing of this reporter produces a GFP signal that can be quantitatively measured by flow cytometry.

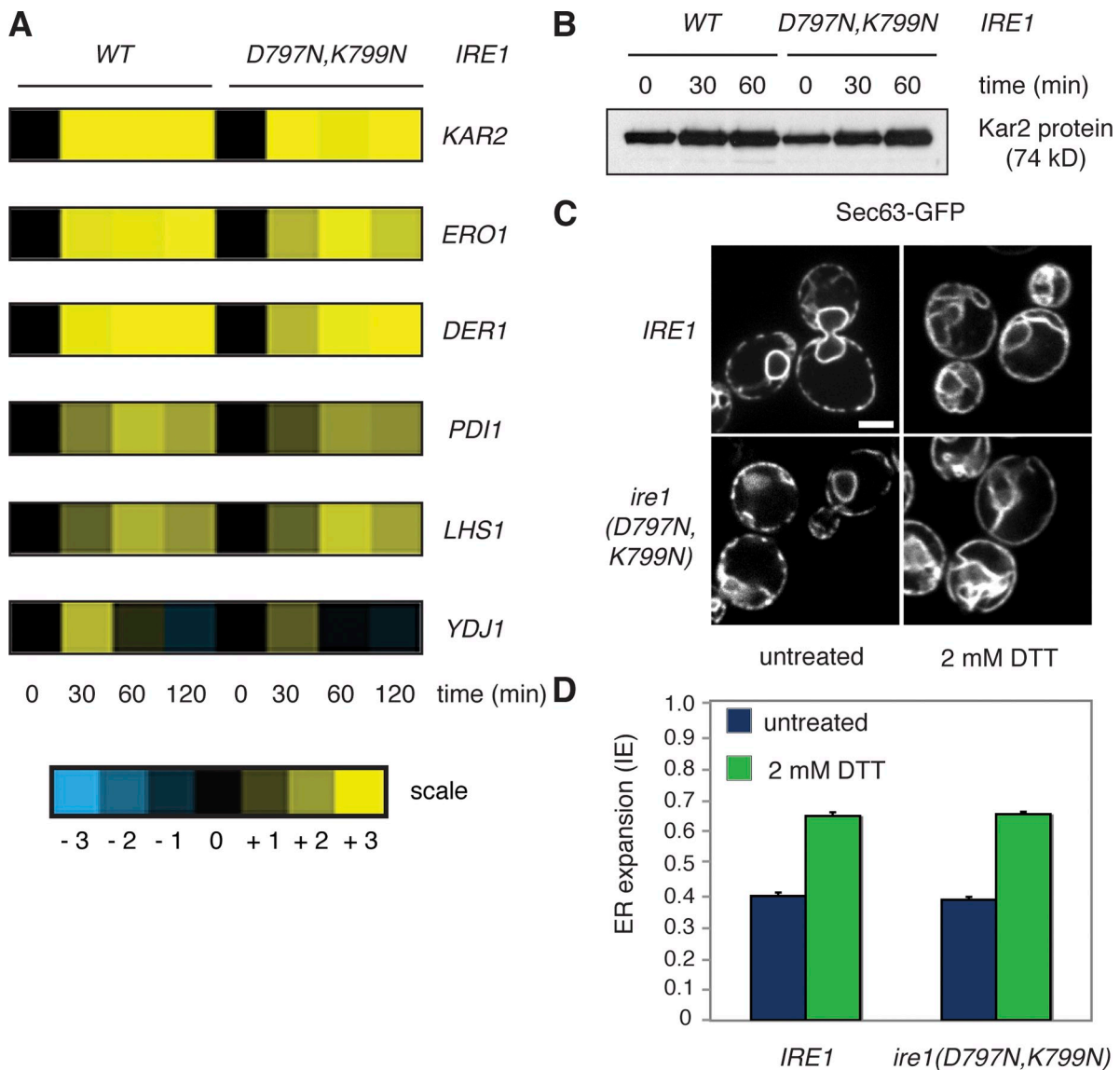


Figure 3. Downstream events in UPR activation are normal in *ire1(D797N,K799N)* cells. (A) Microarray analysis was performed to assess the total mRNA expression profiles of WT *IRE1* or *ire1(D797N,K799N)* cells over time after induction with 2 mM DTT. Cells were sampled at 0, 30, 60, and 120 min. Canonical target genes, *KAR2*, *ERO1*, *DER1*, *PDI1*, and *LHS1* were up-regulated and *YDJ1* was down-regulated equally upon UPR induction in both strains. (B) Total protein was isolated from cells bearing WT *IRE1* or *ire1(D797N,K799N)* after 0, 30, or 60 min in 2 mM DTT and analyzed by Western blot for Kar2 protein. Characteristic increase in Kar2 protein upon UPR induction was observed in both strains. (C and D) ER expansion was measured in WT and *ire1(D797N,K799N)* cells. The UPR was induced in WT or mutant *ire1(D797N,K799N)* cells bearing a GFP-tagged version of Sec63 as an ER marker. Images were taken before and after 2 h UPR induction, and cortical ER expansion was quantified as described in Schuck et al. (2009) and expressed as the index of expansion (IE). Error bars indicate SEM. Bar (C), 2 μ m.

In WT cells, SR fluorescence increased over time with increasing DTT concentration (Fig. 4 B). At low DTT concentrations (below \sim 2 mM), GFP levels in WT cells reached a plateau after \sim 120 min. This plateau, a result of the long half-life of GFP, signifies Ire1 deactivation and is characteristic of an intact homeostatic response that restores the folding capacity of the ER and quells Ire1 signaling.

In *ire1(D797N,K799N)* cells, SR splicing in the first 60–120 min was identical to that observed in WT cells. However, GFP levels continued to rise throughout the time course and its production continued even at doses of DTT to which WT cells adapted (Fig. 4 C). This phenomenon was most evident when reporter activity was plotted as a function of DTT

concentration (Fig. 4, D and E). At the 60-min time point, the dose–response curves for both WT and *ire1(D797N,K799N)* cells overlapped, indicating that GFP production during the activation phase was equivalent for both WT and mutant enzymes (Fig. 4 D). In marked contrast, at 240 min the curves deviated substantially (Fig. 4 E), indicating that after prolonged ER stress *Ire1(D797N,K799N)* continued to signal at low and intermediate doses of DTT. Note that in these experiments both WT *Ire1* and *Ire1(D797N,K799N)* displayed the same basal activity (Fig. 4, D and E; [DTT] = 0.3 mM) and reached the same maximal activity ([DTT] = 3.3 mM), indicating that *Ire1* activation by itself was fully intact in the mutant cells (Fig. S3).

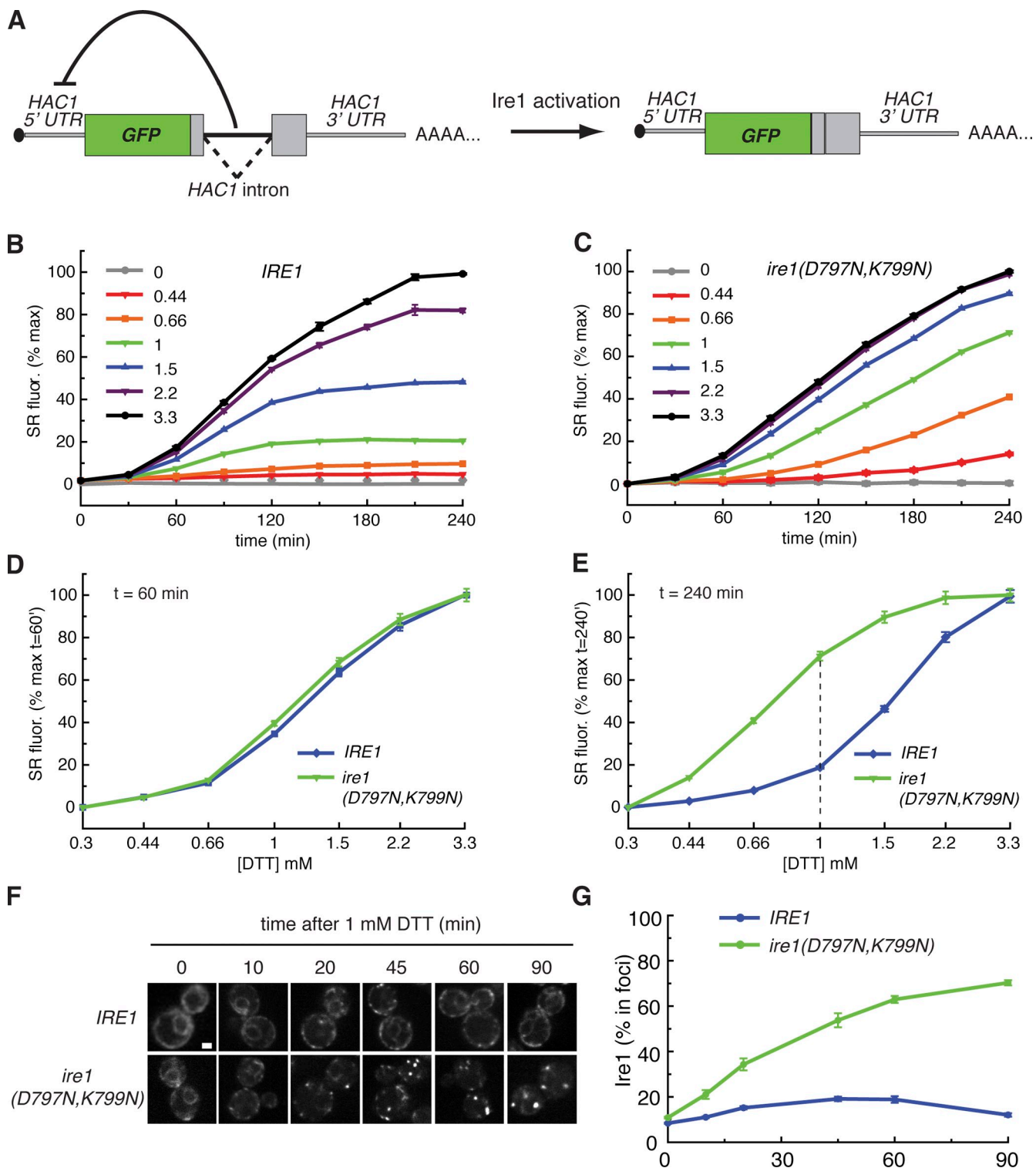


Figure 4. Activation of Ire1(D797N,K799N) continues after WT activity has plateaued. (A) A schematic of the fluorescent splicing reporter (SR) in which the *HAC1* ORF was replaced with GFP such that Ire1-mediated splicing of this reporter produces fluorescent GFP. (B and C) A dilution series of DTT, from 0 to 3.3 mM, was added to cells in culture. WT (B) or *ire1(D797N,K799N)* (C) cells were grown at 30°C and sampled at 30-min intervals over a 4-h time course. GFP signal was measured by flow cytometry, normalized to baseline and plotted over time. (D) SR fluorescence was plotted as a function of increasing [DTT] in WT and *ire1(D797N,K799N)* cells at 60 min after DTT addition. (E) The dose–response of SR fluorescence plotted as a function of [DTT] at 240 min after induction reveals that Ire1(D797N,K799N) was significantly more active than WT at all concentrations of DTT. The dotted line indicates the concentration of DTT at which the two curves most deviated. (F) WT or *ire1(D797N,K799N)* cells bearing GFP-tagged Ire1 were treated with 1 mM DTT and formation of Ire1 foci was imaged by confocal microscopy over time. (G) Foci formation measured in F was quantified as percentage of Ire1 in foci and plotted over time. The maximum value, 100%, is reached when all pixels containing Ire1-GFP signal are in foci (see supplementary methods in Aragón et al., 2009 for a detailed description of quantitation).

As a second measure of Ire1 activity, we monitored Ire1 oligomer formation, which can be observed and quantified by fluorescence microscopy as foci in living cells. Oligomer formation closely correlates with *HAC1* mRNA splicing and therefore is a powerful tool for monitoring Ire1 activation in vivo (Aragón et al., 2009). As in our previous studies, we inserted GFP between the transmembrane linker and kinase domains of WT and mutant forms of Ire1, a location that does not interfere with Ire1 function (Aragón et al., 2009). We measured foci formation of functional WT and mutant Ire1-GFP under conditions at which the adaptation phase dose–response curves of Ire1(D797N,K799N) and WT are most divergent (Fig. 4 E, [DTT] = 1 mM, dotted line). As shown in Fig. 4 F, WT Ire1-GFP formed small, transient foci whereas Ire1(D797N,K799N)-GFP formed foci that persisted to the end of the 90-min experiment (Fig. 4, F and G). This result is consistent with the observation that WT cells adapted to mild ER stress and shut down Ire1 signaling, while Ire1(D797N,K799N)-GFP activation was sustained in the mutant cells. These data indicate that *ire1(D797N,K799N)* cells fail to adapt to prolonged ER stress, suggesting that homeostatic feedback is impaired despite normal induction of UPR target genes.

***Ire1(D797N,K799N)* cells are able to alleviate ER stress**

In principle, the impaired adaptation exhibited in *ire1(D797N,K799N)* cells could be due to a failure of the UPR to fix the problem in the ER or to an inability of Ire1 to deactivate once the stress has been relieved. To test the first possibility, we used a reporter of ER redox potential. DTT induces the UPR by shifting the ER redox potential to become more reducing and causes the accumulation of unfolded proteins by blocking disulfide bond formation; UPR induction, in turn, serves to reoxidize the ER lumen. The level of ER stress can be assessed using an ER-targeted redox-sensitive GFP (ero-GFP) reporter (Hanson et al., 2004; Merksamer et al., 2008). To test whether *ire1(D797N,K799N)* cells restore the oxidizing environment to the ER during sustained UPR insult, cells were treated with 0, 1, or 2 mM DTT (Fig. 5, A and B) and the ratio of reduced/oxidized ero-GFP (“r/o ratio”) was measured by flow cytometry. In WT cells, the ero-GFP r/o ratio increased upon DTT treatment and then gradually decreased as ero-GFP became reoxidized over the course of the experiment (Fig. 5 A).

In *ire1(D797N,K799N)* cells the basal r/o ratio of ero-GFP was elevated relative to that in WT cells (Fig. 5 B, 0 mM DTT) and resulted in a relatively smaller fold increase. Despite the diminished dynamic range of the reporter, reoxidation was evident in *ire1(D797N,K799N)* cells at both concentrations of DTT (Fig. 5 D), indicating that UPR induction restored the oxidative potential of the ER. By contrast, the ero-GFP r/o ratio in *ire1Δ* cells showed normal baseline levels and plateaued after DTT addition (Fig. 5 C). Because these cells are unable to activate the UPR, these data are consistent with the requirement for UPR target gene induction to restore the oxidative environment of the ER.

Deactivation of Ire1(D797N,K799N) is impaired

An unexpected explanation for the elevated baseline of the ero-GFP r/o ratio in *ire1(D797N,K799N)* cells was provided by

observing the intracellular localization of ero-GFP by fluorescence microscopy. In untreated WT cells, ero-GFP was localized to the ER as expected, whereas in *ire1(D797N,K799N)* cells ero-GFP was partially localized to the cytoplasm both before and after UPR induction (Fig. 5 E). The cytosolic ero-GFP likely accounts for the higher basal ero-GFP r/o ratio measured in Fig. 5 B because the cytosol is a reducing environment.

The cytosolic mislocalization of ero-GFP seen in *ire1(D797N,K799N)* cells was puzzling because our preceding data revealed no differences between WT and *ire1(D797N,K799N)* cells in the absence of stress. Most relevantly, mislocalization was not observed for Sec63-GFP, which properly localized to the ER in *ire1(D797N,K799N)* cells (Fig. 3 C). To confirm that translocation of endogenous ER-targeted proteins was normal, we analyzed the translocation of the ER chaperone Kar2. No difference in Kar2 translocation between untreated WT and *ire1(D797N,K799N)* cells was observed (unpublished data). We therefore conclude that the high expression levels of the ero-GFP reporter are responsible for its own localization defect in *ire1(D797N,K799N)* cells. We hypothesize that sustained expression of ER-targeted ero-GFP from a strong constitutive promoter causes chronic ER stress that, in *ire1(D797N,K799N)* cells, interferes with proper ero-GFP import into the ER.

To understand the nature of this ER translocation impairment, we turned to *ire1Δ* cells. These cells, which are unable to mount a productive UPR, properly localized ero-GFP to the ER (Fig. 5 E). The lack of cytosolic ero-GFP signal in *ire1Δ* cells demonstrates that loss of Ire1 activity is not sufficient to impair ER translocation. Rather, a productive UPR is additionally required to cause the translocation defect observed in *ire1(D797N,K799N)* cells.

One possibility is that *ire1(D797N,K799N)* cells fail to adapt to the chronic burden imposed on the ER by ero-GFP expression and do not properly deactivate Ire1. The resulting prolonged UPR signaling would create an overload of ER-targeted proteins, which might overwhelm the capacity of the translocation machinery and cause a back-up of ER client proteins in the cytoplasm. To address this hypothesis, we monitored the abatement of *HAC1* mRNA splicing and resolution of Ire1 foci after removal of ER stress. Northern blot analysis revealed that *HAC1* mRNA splicing in WT cells declined within 45 min of removing DTT and reset by 90 min after DTT removal (Fig. 6 A, top). In contrast, *ire1(D797N,K799N)* cells continued to splice *HAC1* mRNA even 120 min after ER stress had been removed (Fig. 6 A, bottom), indicating that loss of Ire1 kinase activity profoundly delayed Ire1 shut-off. The same trend was observed when we measured Ire1 foci formation: the dissolution of foci in WT cells was noticeable as early as 30 min after DTT washout, whereas Ire1(D797N,K799N) foci were still detectable 120 min after DTT removal (Fig. 6 B). These data are consistent with the hypothesis that the mechanism of Ire1(D797N,K799N) deactivation is impaired despite the fact that protein folding problems inside the ER are alleviated in these cells.

Hyper-phosphorylation of Ire1 is required for rapid de-oligomerization

Mass spectrometry data of the purified cytosolic portion of Ire1 suggest that a 28-amino acid loop (residues 864–892) in the

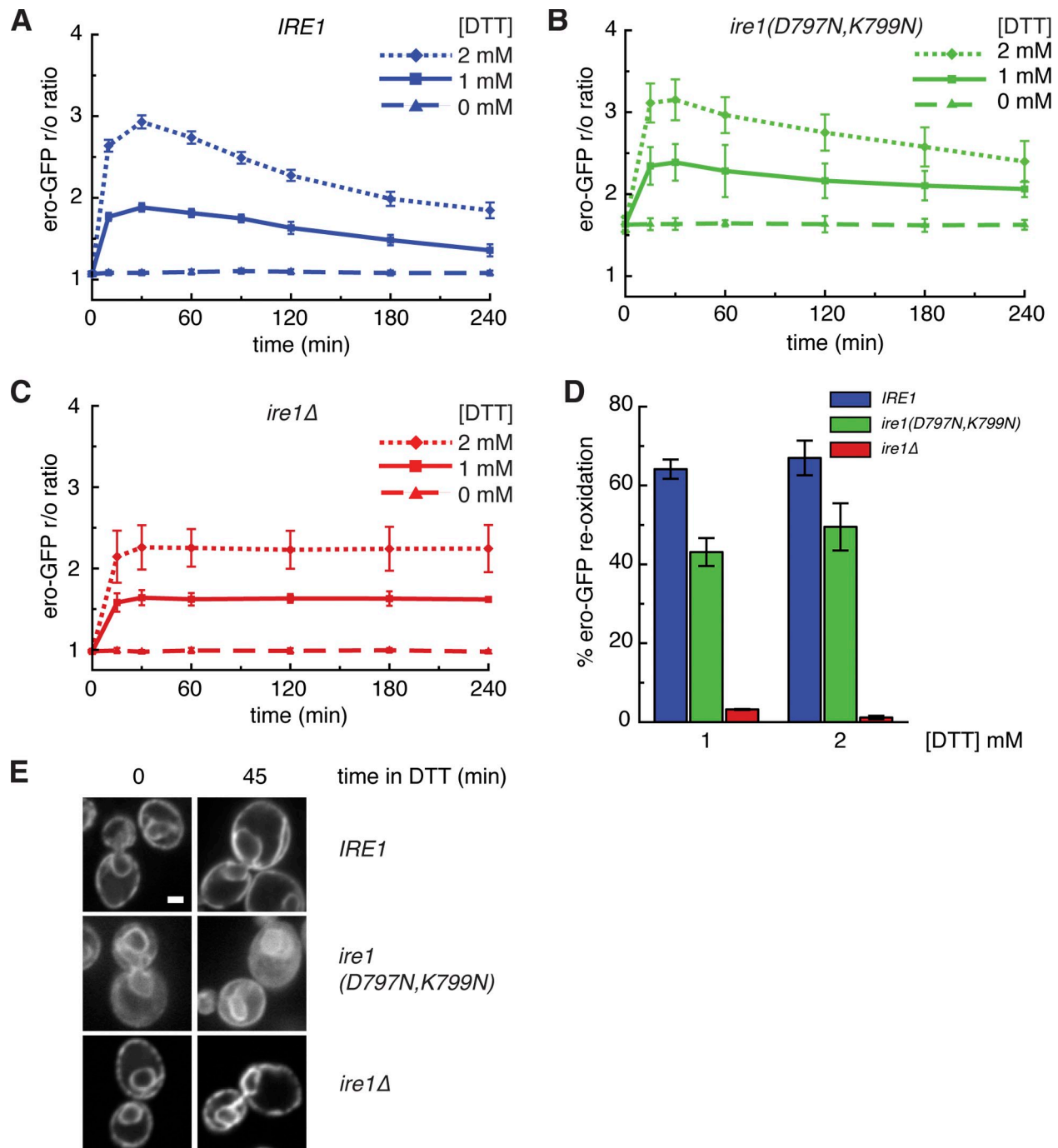


Figure 5. The oxidation potential of the ER is restored in *ire1(D797N,K799N)* cells. (A–D) Re-oxidation of the ero-GFP reporter occurs in the absence of kinase activity. (A) WT, (B) *ire1(D797N,K799N)* and (C) *ire1Δ* cells bearing the ER-targeted redox reporter, ero-GFP, were treated with 0, 1, or 2 mM DTT. The ratio of reduced-to-oxidized signal (r/o ratio) was measured by flow cytometry and plotted over time. (D) Percent reoxidation of ero-GFP was calculated for WT, *ire1(D797N,K799N)*, and *ire1Δ* cells in 0, 1, and 2 mM DTT (see Materials and methods). (E) Cells expressing ero-GFP were analyzed by spinning disk confocal microscopy before and after treatment with 2 mM DTT for 45 min.

C-terminal end of the kinase domain is highly phosphorylated (unpublished data). We propose that trans-autophosphorylation of this loop (termed HPL for hyper-phosphorylated loop) by Ire1 might contribute to quenching Ire1 activity. If this were true, deletion of HPL in WT *IRE1* would mimic the sustained signaling observed in *ire1(D797N,K799N)* cells, whereas deletion of HPL in Ire1(D797N,K799N) would have no effect on the deactivation phenotype of the mutant protein. To test this possibility,

we created *ire1ΔHPL-GFP* and *ire1(D797N,K799N)ΔHPL-GFP* cells and monitored attenuation of Ire1 foci after ER stress removal. As shown in Fig. 6 B, foci in *ire1ΔHPL-GFP* cells formed readily upon treatment with 5 mM DTT and were sustained substantially longer than in WT control cells after DTT was removed. In contrast, the persistence of foci in *ire1(D797N,K799N)ΔHPL-GFP* cells mirrored that in *ire1(D797N,K799N)-GFP* cells (Fig. 6 C, orange and green

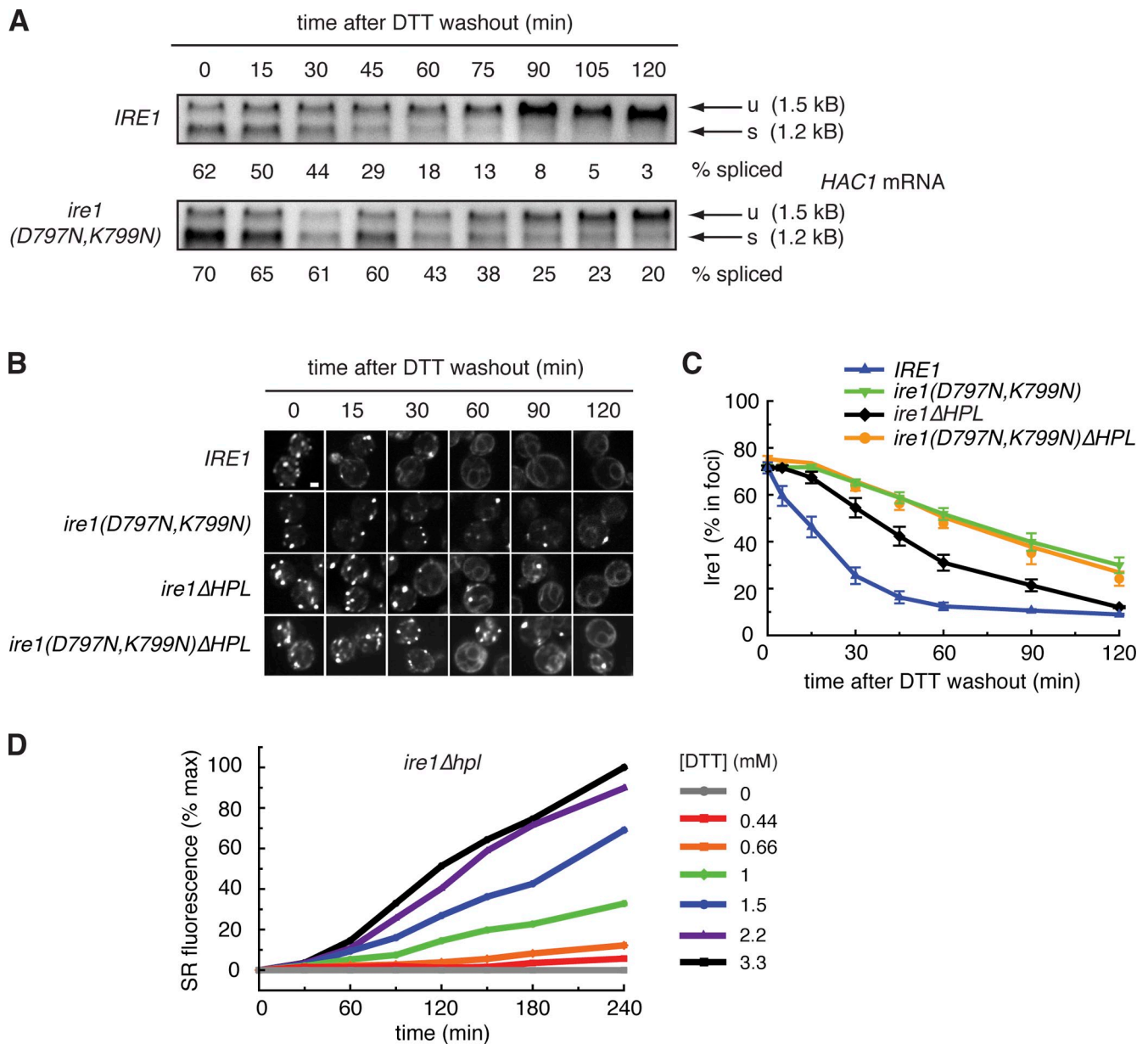


Figure 6. **Shut-off of Ire1(D797N,K799N) is delayed after removal of ER stress.** (A) WT or *ire1(D797N, K799N)* cells were treated with 5 mM DTT for 60 min before DTT washout. Cell samples were taken after DTT washout and total RNA was analyzed by Northern blot for *HAC1* mRNA. Unspliced (u) and spliced (s) forms of *HAC1* mRNA are indicated by arrows. (B and C) GFP-tagged variants of Ire1 were visualized by fluorescence microscopy after washout of 5 mM DTT. Quantitation of Ire1 foci is displayed in the bottom panel. (D) *Ire1ΔHPL* cells retain RNase activity. A dilutions series of DTT, from 0 to 3.3 mM, was added to *ire1ΔHPL* cells bearing the splicing reporter, SR. Cells were grown at 30°C and sampled at 30-min intervals over a 4-h time course. GFP signal was measured by flow cytometry and plotted over time.

lines), indicating that deletion of HPL had no effect on deactivation of Ire1 in the absence of phosphoryl-transfer. Importantly, *ire1ΔHPL-GFP* cells retained RNase activity as measured by SR splicing (Fig. 6 D), indicating that activation of Ire1ΔHPL-GFP was intact. Interestingly, the SR splicing phenotype of *ire1ΔHPL-GFP* cells resembled that of *ire1(D797N,K799N)* cells, indicating that Ire1ΔHPL has a deactivation defect similar to kinase-inactive Ire1 (compare Figs. 4 C and 6 D). The kinetics of foci disappearance in *ire1ΔHPL* cells resembled that in *ire1(D797N,K799N)* cells (Fig. 6 B), supporting the hypothesis that the HPL contributes to the regulation of Ire1 shut-off. Notably, however, the phenotype in *ire1ΔHPL* cells was not as

strong as that seen in *ire1(D797N,K799N)* cells, indicating that phosphorylation of regions outside the HPL must also contribute to Ire1 deactivation.

Discussion

Ire1 provides the central gate in the information flow from the ER lumen during UPR induction. In response to sensing excessive concentrations of mis- or unfolded proteins in the ER lumen, Ire1 undergoes oligomerization and activation of its RNase function, which initiates the nonconventional splicing of *HAC1* mRNA. The role of Ire1's kinase domain has remained mysterious.

The paradox primarily derives from the observation that phosphoryl-transfer can be entirely bypassed in drug-sensitized Ire1 mutants while splicing and the downstream transcriptional program remain active, yet other mutations in the kinase domain, such as K702R, which abolishes kinase activity, impair the UPR. Here we used a rationally designed mutation in the kinase-active site that blocks phosphoryl-transfer activity but preserves nucleotide binding. The mutant retains Ire1's activation potential *in vivo*. Despite activating the canonical set of UPR target genes, however, the mutation prevents cells from restoring homeostasis. We trace this physiological defect to a defect in Ire1 shut-off, revealing a role of Ire1-mediated phosphoryl-transfer in regulating the homeostatic feedback of the UPR that is important for cell survival. A recent independent study (see Chawla et al. in this issue) showed that kinase-inactive Ire1(D828A) was able to bind nucleotide cofactor but was likewise unable to shut down Ire1 signaling in the absence of kinase activity. These data lend further support to the notion that Ire1 kinase plays an important role in the attenuation of Ire1 signaling.

Ire1 mutations allow uncoupling of kinase and RNase activities

Occupancy of the nucleotide-binding pocket in the Ire1 kinase domain renders the cytosolic portion of Ire1 prone to oligomerization by stabilizing the kinase module in the open conformation (Korennykh et al., 2009). Oligomerization in turn causes activation of Ire1's RNase, as interactions between neighboring Ire1 molecules in the ordered oligomer stabilize essential structural elements in the RNase-active site (Korennykh et al., 2009). Conformational control of the Ire1 kinase domain therefore regulates RNase activation.

In the ER membrane, oligomerization of Ire1 luminal domains triggers activation of Ire1's cytosolic kinase/RNase modules by increasing their local concentration. In this manner, Ire1's RNase activity is subservient to events in the ER lumen, and cofactor binding to the kinase domain adjusts the activation threshold of the enzyme. Despite being kinase inactive, we found that Ire1(D797N,K799N) preserves activation of the UPR. The RNase activity of Ire1KR32(D797N,K799N) is responsive to the addition of nucleotide *in vitro* and Ire1(D797N,K799N) retains ER stress-responsive RNase activity *in vivo*, suggesting that nucleotide binding is a key step in Ire1 activation. Recent work showed that the nucleotide-binding pocket of Ire1 kinase was highly conserved in a sequence comparison of yeast Ire1 species, further supporting the notion that this binding module is an essential component of Ire1 (Poothong et al., 2010).

Sustained production of ER-targeted proteins is detrimental

We found that Ire1(D797N,K799N) activity is sustained well beyond the time when WT Ire1 activity shuts off, illustrating a loss in the quality of the UPR homeostatic feedback regulation. While ER stress properly activates Ire1(D797N,K799N) and induces a canonical transcriptional response, the mutant enzyme continues to signal as though the response were ineffective. Thus, the kinase activity of Ire1 plays a crucial role in completing the negative feedback loop of the UPR.

In WT cells, ero-GFP is localized to the ER and can serve as a reporter of the ER environment. Despite inducing the canonical UPR transcriptional program, *ire1(D797N,K799N)* cells exclude a portion of ero-GFP from the ER. In this context, a fraction of the reporter is retained in the reducing environment of the cytosol and ero-GFP returns a misleading signal that does not properly report on the condition of the ER lumen. Results obtained with this reporter must therefore be interpreted with caution. We believe that despite the increased baseline r/o ratio measured in *ire1(D797N,K799N)* cells, oxidative folding conditions are restored in the ER lumen. We surmise that the increase in cytosolic signal of ero-GFP is due to impaired ER translocation of the reporter.

The simplest explanation for this translocation block is that an increased load of ER-targeted proteins resulting from sustained activation of the UPR overloads the import machinery. In accordance with this view, long-term, acute ER stress leads to the appearance of preKar2 protein in WT cells as well, where it was previously observed as a higher molecular weight band (e.g., see Fig. 5 A in Schuck et al., 2009). Thus, it appears that the capacity of a cell to adapt to the increased ER load on the ER translocation machine may be inherently limited, leading to protein mislocalization under conditions of extreme stress. In this scenario, an ER-translocation defect would be a symptom of severe ER stress and may be coupled to a plethora of pleiotropic defects that could explain the severe growth defect observed in UPR-induced *ire1(D797N,K799N)* cells.

In mammalian cells, activation of the PERK-branch of the UPR serves to down-regulate translation and thereby to reduce the overall load of newly synthesized proteins entering the ER. In *S. cerevisiae* no analogous pathway exists. The PERK pathway might have evolved as a solution to the impairment in ER translocation observed in yeast and therefore serves a physiologically desirable function: to slow the influx of protein into the secretory pathway under conditions of ER stress.

Phosphorylation of Ire1 is important for deactivation

A compelling finding in this work is that phosphoryl-transfer by Ire1 kinase, although largely dispensable for its activation, plays an important role in Ire1 shut-off. Abatement of *HAC1* mRNA splicing and dispersal of foci are delayed in *ire1(D797N,K799N)* mutant cells, both under mild ER stress where the UPR in WT cells can restore homeostasis and under massive ER stress followed by washout of the inducing agent. Here we postulate that phosphorylation of Ire1 contributes significantly to its deactivation. We propose that without phosphorylation to aid in Ire1 de-oligomerization, Ire1(D797N,K799N) shut-off occurs by diffusional dispersion upon oligomer dissociation. Although the molecular mechanism by which phosphorylation promotes Ire1 shut-off is currently not understood, we have shown that a 28-amino acid surface loop (HPL) on the Ire1 kinase domain is important for efficient shut down of Ire1 signaling. Because deletion of the HPL from Ire1 only partially phenocopies the *D797N,K799N* mutation, it is likely that other regions in Ire1 also contribute. The HPL contains seven serine and two threonine residues that could be phosphorylated. Peptides corresponding

to this loop are selectively missing from mass spectrometry analyses of recombinant, phosphorylated Ire1KR32, yet can be detected after phosphatase treatment (unpublished data). Because phosphopeptides are notoriously difficult to detect by mass spectrometry, these data suggest that peptides in this loop are phosphorylated. Deletion of the HPL from a recombinant Ire1 construct, Ire1KR32 Δ 28, was necessary in order to yield a high-resolution crystal structure of active oligomeric Ire1 (Korennykh et al., 2009). These observations lead us to speculate that the HPL is highly phosphorylated and destabilizes oligomerization of the cytosolic portion of Ire1 in vitro, perhaps by charge repulsion. A similar mechanism might operate in vivo, with phosphorylation of the HPL contributing to dissolution of Ire1 oligomers and thereby to Ire1 deactivation. Alternatively, some still-unknown UPR-modulating protein might bind the phosphorylated HPL and, akin to arrestin binding to G protein-coupled receptors, coordinate timely shut-off of Ire1 signaling. In addition, it remains possible that Ire1 kinase has other, yet-unidentified, targets that promote cell survival when phosphorylated.

Demonstrating a role of Ire1 phosphorylation in its shut-off does not contradict the notion that phosphorylation events also play a role in its activation. In particular, we have previously shown that phosphorylated residues in Ire1's activation loop form salt bridges to adjacent Ire1 subunits in the active oligomer (Korennykh et al., 2009). The mild hypomorphic effects on *HAC1* mRNA splicing observed in *ire1(D797N,K799N)* cells may result from a lack of such positive feedback that enhances oligomer stability initially through phosphorylation.

Destabilization of Ire1 oligomers by phosphorylation of the HPL and other sites may be temporally delayed and serve as a molecular timer that balances oligomer assembly and disassembly. In this scenario, both forward and reverse reactions would remain responsive to changing conditions in the ER lumen and the Ire1 signal transmitted via the oligomerization state of the luminal domain. Longer Ire1 activity would lead to the accumulation of a greater number of phosphates and an Ire1 oligomer would be

increasingly destabilized. In this way, phosphorylation may aid the rapid disassembly even of large oligomers that are held together through multiple, mutually reinforcing intramolecular interactions. The luminal domain of Ire1 would thus remain empowered as the sole driver of activation and de-activation, thereby rendering Ire1 highly sensitive to changes in the ER lumen.

Materials and methods

Yeast strains and growth conditions

Cells were grown in 2x synthetic complete medium supplemented with 100 μ g/ml inositol. Over the course of this study, we noticed that Ire1 kinase-inactive cells were sensitive to saturation in culture. Thus, cells grown in culture were kept at subsaturating conditions for at least 12 h before beginning any experiment. The yeast strains and plasmids used in this study are listed in Tables I and II, respectively.

In vitro assays

Recombinant Ire1 proteins were purified from *E. coli* as described previously (Korennykh et al., 2009).

Kinase assays were performed using 10 μ M of purified Ire1 in kinase buffer (20 mM Hepes, pH 7.0 at 30°C, 70 mM NaCl, 2 mM Mg(OAc)₂, 5 mM DTT, and 5% glycerol) supplemented with 0.033 μ M [γ -³²P]-ATP (Perkin-Elmer). Reactions were performed at 30°C. In reactions containing two distinct versions of recombinant Ire1 protein, 5 μ M of each was added. Phosphorylated proteins were separated on a 12% denaturing polyacrylamide gel and detected with a phosphorimager screen (Molecular Dynamics).

MALDI mass spectrometry and in vitro RNA cleavage assays were performed as described by Korennykh et al. (2009). In vitro cleavage reactions were started by adding 1 μ l of ³²P-labeled RNA to 9 μ l of premixture containing 20 mM Hepes, pH 7.4, 70 mM NaCl, 2 mM MgCl₂, 4 mM DTT, 5% glycerol, and 2 mM ADP. Reactions were performed at 30°C, contained \leq 1 pM radioactively ³²P-labeled RNA, 3 μ M purified Ire1, and were conducted under single turnover conditions. Reactions were quenched at time intervals with 6 μ l stop solution (10 M urea, 0.1% SDS, 0.1 mM EDTA, 0.05% xylene cyanol, and 0.05% bromophenol blue). Samples were analyzed by 10–20% PAGE, gels were scanned by Typhoon (Molecular Dynamics), and quantified using ImageQuant and GelQuant.NET programs. The data were plotted and fit to exponential curves using SigmaPlot to determine observed rate constants.

Isolation of total RNA and Northern blot analysis

Total RNA was isolated from yeast cells using hot acid phenol chloroform extraction (Rüegsegger et al., 2001). Unless otherwise indicated, the UPR was induced by the addition of 2 mM DTT (Gold Biotechnology) for 40 min.

Table I. Yeast strains

Yeast strain	Genotype
YCR200	<i>ire1Δ::TRP1, his3::UPRE-LACZ-HIS3, W303a derivative</i>
YCR201	as YCR200, except <i>ura3::IRE1-3xFLAG-URA3</i>
YCR202	as YCR200, except <i>ura3::ire1(D797N, K799N)-3xFLAG-URA3</i>
YCR203	as YCR200, except <i>ura3::ire1(D828A)-3xFLAG-URA3</i>
YDP002	<i>cry1a, ire1::KanMX6 [23]</i>
YCR204	as YDP002, except <i>ura3::IRE1-3xFLAG</i>
YCR205	as YDP002, except <i>ura3::ire1(D797N, K799N)-3xFLAG</i>
YCR206	as YDP002, except <i>ura3::IRE1-3xFLAG, his3::HA-HAC1-HIS3</i>
YCR207	as YDP002, except <i>ura3::ire1(D797N, K799N)-3xFLAG, his3::HA-HAC1-HIS3</i>
YCR208	as YDP002, except <i>IRE1-3xFLAG, leu2::SR-LEU2</i>
YCR209	as YDP002, except <i>ire1(D797N, K799N)-3xFLAG, leu2::SR-LEU2</i>
YCR210	as YCR201, except <i>TDH3::ero-GFP-kanMX6-4xUPRE-mCherry</i>
YCR211	as YCR202 except <i>TDH3::ero-GFP-kanMX6-4xUPRE-mCherry</i>
YCR212	as YDP002, except <i>leu2::IRE1-GFP-LEU2</i>
YCR213	as YDP002, except <i>leu2::ire1(D797N, K799N)-GFP-LEU2</i>
YCR214	as YDP002, except <i>leu2::ire1(D828A)-GFP-LEU2</i>
YCR215	as YDP002, except <i>leu2::ire1ΔHPL-GFP-LEU2</i>
YCR216	as YDP002, except <i>leu2::ire1(D797N, K799N)ΔHPL-GFP-LEU2</i>

Northern blot analysis was performed using 15 µg of total RNA separated on a 1.5% (wt/vol) denaturing agarose gel and transferred to a supported nitrocellulose membrane (GE Water & Press Technologies). The *HAC1* mRNA was detected using a radiolabeled 500-bp DNA probe directed against the 5' exon of the transcript (Cox and Walter 1996).

Cell viability assays

To score the plate phenotype, yeast cells were grown to an OD₆₀₀ of 0.3 or lower and diluted to equal cell numbers. Cell suspensions were serially diluted 1:5 and transferred to plates using a pin tool. UPR-inducing plates contained 0.25 µg/ml tunicamycin (EMD). To analyze cell viability in culture, cells were grown in the presence of 2 mM DTT at 30°C for 26 h. At each time point, cells were counted, the OD₆₀₀ was measured, and 300 cells were plated onto permissive media. Colony forming units (CFUs) were counted from the plates after 3 d at 30°C. Viability was calculated by dividing the number of CFUs by the number of cells plated. Cells were kept below an OD₆₀₀ of 0.2 and the DTT was refreshed throughout the course of the experiment.

Isolation of protein and Western blot analysis

Total protein was isolated from cells by vortexing in the presence of glass beads in 8 M urea, 50 mM Hepes, pH 7.4, and 1% SDS. Samples were boiled then cleared by centrifugation at 16,000 g for 10 min. 25 µg total protein was separated by SDS-PAGE (NuPAGE; Invitrogen), transferred to nitrocellulose, and probed with antibody. For HA-epitope detection, the monoclonal HA.11 (Covance) was used at a dilution of 1:3,000. Pgk1 protein was detected using Pgk1-specific antibody at a 1:5,000 dilution (Invitrogen). For detection of the Kar2 protein, a Kar2-specific antibody (Walter laboratory, University of California, San Francisco, San Francisco, CA) was used at a 1:5,000 dilution.

Microarray analysis

Cultures were inoculated to an OD₆₀₀ of 0.05 and grown at 30°C in 2x synthetic media supplemented with 100 µg/ml inositol. Upon reaching an OD₆₀₀ of 0.3, the UPR was induced by the addition of 2 mM DTT. Cells were harvested at 0, 30, 60, and 120 min from 500 ml of culture (150 ODs) by filtration onto a nitrocellulose membrane (Millipore). Membranes were frozen in liquid nitrogen and stored at -80°C before RNA isolation.

Total RNA was isolated using hot acid phenol chloroform extraction (Sarver and DeRisi 2005). cDNA was reverse transcribed from 15 µg of total RNA using Superscript III (Invitrogen) and a 1:1 mixture of oligo(dT) and random hexamers. Reverse transcription was performed in the presence of amino-allyl dUTP (aa-dUTP) (Invitrogen) at a ratio of 2:3 aa-dUTP/dTTP. A fraction of each cDNA sample was pooled to create a reference sample; the pooled reference was labeled with Cy3 dye (GE Healthcare). The remaining sample cDNA from each time point was labeled with Cy5 dye (GE Healthcare). Each Cy5-labeled sample was mixed with an equal amount of Cy3-labeled pooled reference cDNA and hybridized to oligonucleotide microarrays representing the full yeast genome (DeRisi et al., 1997). Microarray data were extracted and analyzed using the methods described in Sarver and DeRisi (2005). Before clustering, data were compressed such that all data corresponding to identical gene products were averaged.

Yeast oligonucleotide arrays were printed using primers for each predicted or known gene supplied by Operon. Two primer sets, AROS and YBOX, were combined to create these arrays. Oligonucleotide arrays were printed at the UCSF Center for Advanced Technology (San Francisco, CA).

Measuring global translation rates and ER expansion

Global translation rates were measured by monitoring [³⁵S]methionine incorporation during UPR induction. Cells were grown to an OD₆₀₀ of 0.3, harvested by filtration, and resuspended in media lacking methionine.

Starvation was performed for 30 min at 30°C. The UPR was induced by the addition of 2 mM DTT. At the time of UPR induction, 1 µCi/ml [³⁵S]methionine (PerkinElmer) plus 50 µM cold methionine was added to cells. The OD₆₀₀ was measured and samples were harvested every 15 min for 3 h after UPR induction. Cells were lysed, total protein was isolated by TCA precipitation, and scintillation counts were measured. To graph the results, total scintillation counts were normalized to the OD₆₀₀ and plotted over time.

To assay ER expansion, WT or mutant *ire1* cells bearing *SEC63-GFP* on a centromeric plasmid were left untreated or treated with 2 mM DTT for 2 h and imaged. Expansion of the cortical ER was quantified as described previously (Schuck et al., 2009). In brief, we first measured the Sec63-GFP signal along the cell cortex for at least 40 cells per condition and calculated its coefficient of variation (CV). The cortical ER of untreated cells appears as a broken line with large signal fluctuations, giving a high CV. In DTT-treated cells, Sec63-GFP is more evenly distributed along the cell cortex as part of expanded ER sheets, resulting in a low CV. We then derived the index of expansion (IE) by dividing the CV of the Sec63-GFP signal from the nuclear envelope, which represents maximally expanded ER and yields the smallest possible CV, by the CV of the cortical signal. Hence, the IE increases as the ER expands.

Splicing reporter (SR) assays

WT or mutant cells bearing SR integrated at the *URA3* locus were induced with DTT as indicated and flow cytometry was performed as described previously (Pincus et al., 2010). Cells were cultured at 30°C in 2x SDC in 96-well deep-well plates in a plate shaker (Innova) at 900 rpm. 1 M DTT stocks were made fresh from powder and stored at 4°C for each experiment. Fresh 5x working stocks were prepared at the start of the experiment by diluting DTT in 1 step into 2x SDC to 37.5 mM (5x 7.5 mM) in 10 ml. This 37.5-mM working stock was serially diluted by 1.5-fold increments (6 ml + 3 ml SDC) 10 times to span the range. To initiate the experiment, 200 µl of each 5x stock was added to 800 µl cells in the 96-well plates at time 0. Cells were incubated at 30°C and sampled every 30 min by 12-channel pipetting 100 µl of each culture into a 96-well microtiter plate. 10 µl of each 100 µl was sampled to flow cytometry analysis using a flow cytometer (model LSR-II; BD) equipped with a high throughput sampler, a 488-nm 100-mW laser, FITC emission filter, and FACS DIVA software to compile .fcs files. Files were analyzed in MatLab and/or Flajo. No cuts or gates were applied to cell distributions. Median FITC-A values were calculated for each dose-time point and plotted in ProFit. Errors were calculated from the standard deviation of the median for three biological replicates.

Measuring the redox potential of the ER using the ero-GFP reporter

To measure the ER redox potential the ero-GFP reporter (pPM56; Merksamer et al., 2008) was integrated into the *TDH3* locus of WT or mutant cells. The UPR was induced with 1 mM or 2 mM DTT. GFP fluorescence at 405 nm and 488 nm was measured by flow cytometry and the ratio of the 405-nm and 488-nm signal (*r/o* ratio) was plotted as a function of time. Percent ero-GFP reoxidation was calculated using the equation: % reoxidation = $1 - ((F - I)/(M - I))$ where *I* = initial ero-GFP *r/o* ratio (at *t* = 0), *M* = maximum ero-GFP *r/o* ratio (at *t* = 30 min), and *F* = final ero-GFP *r/o* ratio (at *t* = 240 min).

Ire1 foci formation and quantitative fluorescence microscopy

IRE1 was tagged with *GFP* as described previously (Aragón et al., 2009) and integrated at the *LEU2* locus to create strains YCR212, YCR213, and YCR214. Cells were grown in an Erlenmeyer flask at 30°C and transferred to a 96-well glass-bottom plate coated with concanavalin A. Ire1-GFP was imaged by confocal microscopy and images were processed and quantified as described by Pincus et al. (2010). Microscopy was performed

Table II. Yeast plasmids

Plasmid	Description	Marker
pCR100	<i>IRE1-3xFLAG</i> , pRS306	URA3
pCR101	<i>ire1</i> (D797N, K799N)-3xFLAG, pRS306	URA3
pCR102	<i>ire1</i> (D828A)-3xFLAG, pRS306	URA3
pCR103	<i>IRE1-3xFLAG</i> , pRS303	HIS3
pCR104	<i>ire1</i> (D797N, K799N)-3xFLAG, pRS303	HIS3
pPM56	<i>TDH3-ero-GFP</i> , 4xUPRE-mCherry (Merksamer et al., 2008)	URA3, kanMX6
pJK59	<i>Sec63-GFP</i> , CEN (Prinz et al., 2000)	URA3

using a spinning disk confocal unit (CSU-22; Yokogawa) on a TI inverted microscope (Nikon) equipped with a 150-mW, 491-nm laser and an EMCCD camera (Evolve; Photometrics). Cells were grown in 2x SDC to mid-log phase, diluted to $OD_{600} = 0.1$, gently sonicated, and 80 μ l was added to 96-well glass-bottom plates coated with concanavalin A. Cells were allowed to settle for 20 min before imaging. DTT was prepared as 5x working stocks as in flow cytometry SR assays, and 20 μ l added to wells at time 0. For washout experiments, cells were incubated with 5 mM DTT for 1 h in Eppendorf tubes and washed 2x with fresh media before transferring to 96-well plates for imaging. Cells were imaged at each time point using a 100x oil objective with 5-s exposures of 491-nm excitation. Images were acquired using the open source MicroManager v1.2 software, processed by identifying cell boundaries and assigning the 16-bit fluorescence images to individual cells using the open source Cell-ID software. Background was calculated from the mean intensity of areas in each fluorescent image not assigned to cells, and subtracted from the cellular mean intensities to obtain corrected single-cell values. For each time point at each dose, images of three different fields of cells were obtained and quantified. Thus, a total of 30–100 cells were analyzed per time point. Mean values were plotted in ProFit and error bars represent the standard error of the mean.

Online supplemental material

Fig. S1 shows that mutations in Ire1 kinase abolish phosphoryl-transfer. Fig. S2 shows that the transcriptional response and global translation rates are normal in *ire1(D797N,K799N)* cells. Fig. S3 shows that the fold change of SR splicing in WT and *ire1(D797N,K799N)* cells are comparable. Online supplemental material is available at <http://www.jcb.org/cgi/content/full/jcb.201007077/DC1>.

The authors wish to thank Joe DeRisi, the UCSF Center for Advanced Technology (CAT), and Philipp Kimmig for reagents and assistance with the microarray hybridization experiments; and Kurt Thorn and the Nikon Imaging Center (NIC) as well as the Consortium for Frontotemporal Dementia Research (CFR) for assistance with and access to spinning disk confocal microscopes. We are grateful to Christopher Patil, Shannon Behrman, and Saskia Neher for critical reading of the manuscript and to Jonathan Weissman, Joe DeRisi, and members of the Walter Laboratory for expert advice and valuable discussion throughout the course of the project. We thank Will Prinz and Phillip Merksamer for providing plasmids.

C. Rubio was supported by the National Science Foundation and the UC President's Dissertation Year Fellowship; D. Pincus was supported by the National Science Foundation; A. Korennykh was supported by the Jane Coffin Childs Memorial Fund for Medical Research Fellowship; and S. Schuck was supported by the Human Frontier Science Program. Research was additionally funded by grants from the National Institutes of Health to P. Walter and H. El-Samad, and the Howard Hughes Medical Institute. P. Walter is an Investigator of the Howard Hughes Medical Institute.

The authors declare no conflicts of interest.

Submitted: 15 July 2010

Accepted: 1 February 2011

References

- Aragón, T., E. van Anken, D. Pincus, I.M. Serafimova, A.V. Korennykh, C.A. Rubio, and P. Walter. 2009. Messenger RNA targeting to endoplasmic reticulum stress signalling sites. *Nature*. 457:736–740. doi:10.1038/nature07641
- Bernales, S., K.L. McDonald, and P. Walter. 2006. Autophagy counterbalances endoplasmic reticulum expansion during the unfolded protein response. *PLoS Biol.* 4:e423. doi:10.1371/journal.pbio.0040423
- Bertolotti, A., Y. Zhang, L.M. Hendershot, H.P. Harding, and D. Ron. 2000. Dynamic interaction of BiP and ER stress transducers in the unfolded-protein response. *Nat. Cell Biol.* 2:326–332. doi:10.1038/35014014
- Chawla, A., S. Chakrabarti, G. Ghosh, and M. Niwa. 2011. Attenuation of the yeast UPR response is essential for survival and is mediated by IRE1 kinase. *J. Cell Biol.* 193:41–50. doi:10.1083/jcb.201008071
- Cox, J.S., and P. Walter. 1996. A novel mechanism for regulating activity of a transcription factor that controls the unfolded protein response. *Cell*. 87:391–404. doi:10.1016/S0092-8674(00)81360-4
- Cox, J.S., C.E. Shamu, and P. Walter. 1993. Transcriptional induction of genes encoding endoplasmic reticulum resident proteins requires a transmembrane protein kinase. *Cell*. 73:1197–1206. doi:10.1016/0092-8674(93)90648-A
- Cox, J.S., R.E. Chapman, and P. Walter. 1997. The unfolded protein response coordinates the production of endoplasmic reticulum protein and endoplasmic reticulum membrane. *Mol. Biol. Cell.* 8:1805–1814.
- Credle, J.J., J.S. Finer-Moore, F.R. Papa, R.M. Stroud, and P. Walter. 2005. On the mechanism of sensing unfolded protein in the endoplasmic reticulum. *Proc. Natl. Acad. Sci. USA*. 102:18773–18784. doi:10.1073/pnas.0509487102
- DeRisi, J.L., V.R. Iyer, and P.O. Brown. 1997. Exploring the metabolic and genetic control of gene expression on a genomic scale. *Science*. 278:680–686. doi:10.1126/science.278.5338.680
- Dong, B., M. Niwa, P. Walter, and R.H. Silverman. 2001. Basis for regulated RNA cleavage by functional analysis of RNase L and Ire1p. *RNA*. 7:361–373. doi:10.1017/S1355838201002230
- Hanson, G.T., R. Aggeler, D. Oglesbee, M. Cannon, R.A. Capaldi, R.Y. Tsien, and S.J. Remington. 2004. Investigating mitochondrial redox potential with redox-sensitive green fluorescent protein indicators. *J. Biol. Chem.* 279:13044–13053. doi:10.1074/jbc.M312846200
- Kimata, Y., D. Oikawa, Y. Shimizu, Y. Ishiwata-Kimata, and K. Kohno. 2004. A role for BiP as an adjustor for the endoplasmic reticulum stress-sensing protein Ire1. *J. Cell Biol.* 167:445–456. doi:10.1083/jcb.200405153
- Korennykh, A.V., P.F. Egea, A.A. Korostelev, J. Finer-Moore, C. Zhang, K.M. Shokat, R.M. Stroud, and P. Walter. 2009. The unfolded protein response signals through high-order assembly of Ire1. *Nature*. 457:687–693. doi:10.1038/nature07661
- Lee, K.P., M. Dey, D. Neculai, C. Cao, T.E. Dever, and F. Sicheri. 2008. Structure of the dual enzyme Ire1 reveals the basis for catalysis and regulation in nonconventional RNA splicing. *Cell*. 132:89–100. doi:10.1016/j.cell.2007.10.057
- Merksamer, P.I., A. Trusina, and F.R. Papa. 2008. Real-time redox measurements during endoplasmic reticulum stress reveal interlinked protein folding functions. *Cell*. 135:933–947. doi:10.1016/j.cell.2008.10.011
- Mori, K., W. Ma, M.J. Gething, and J. Sambrook. 1993. A transmembrane protein with a cdc2+/CDC28-related kinase activity is required for signaling from the ER to the nucleus. *Cell*. 74:743–756. doi:10.1016/0092-8674(93)90521-Q
- Mori, K., T. Kawahara, H. Yoshida, H. Yanagi, and T. Yura. 1996. Signalling from endoplasmic reticulum to nucleus: transcription factor with a basic-leucine zipper motif is required for the unfolded protein-response pathway. *Genes Cells*. 1:803–817. doi:10.1046/j.1365-2443.1996.d01-274.x
- Okamura, K., Y. Kimata, H. Higashio, A. Tsuru, and K. Kohno. 2000. Dissociation of Kar2p/BiP from an ER sensory molecule, Ire1p, triggers the unfolded protein response in yeast. *Biochem. Biophys. Res. Commun.* 279:445–450. doi:10.1006/bbrc.2000.3987
- Papa, F.R., C. Zhang, K. Shokat, and P. Walter. 2003. Bypassing a kinase activity with an ATP-competitive drug. *Science*. 302:1533–1537. doi:10.1126/science.1090031
- Pincus, D., M.W. Chevalier, T. Aragón, E. van Anken, S.E. Vidal, H. El-Samad, and P. Walter. 2010. BiP binding to the ER-stress sensor Ire1 tunes the homeostatic behavior of the unfolded protein response. *PLoS Biol.* 8:e1000415. doi:10.1371/journal.pbio.1000415
- Poohong, J., P. Sopha, R.J. Kaufman, and W. Tirasophon. 2010. Domain compatibility in Ire1 kinase is critical for the unfolded protein response. *FEBS Lett.* 584:3203–3208. doi:10.1016/j.febslet.2010.06.003
- Prinz, W.A., L. Grzyb, M. Veenhuis, J.A. Kahana, P.A. Silver, and T.A. Rapoport. 2000. Mutants affecting the structure of the cortical endoplasmic reticulum in *Saccharomyces cerevisiae*. *J. Cell Biol.* 150:461–474. doi:10.1083/jcb.150.3.461
- Rüegsegger, U., J.H. Leber, and P. Walter. 2001. Block of HAC1 mRNA translation by long-range base pairing is released by cytoplasmic splicing upon induction of the unfolded protein response. *Cell*. 107:103–114. doi:10.1016/S0092-8674(01)00505-0
- Sarver, A., and J. DeRisi. 2005. Fzf1p regulates an inducible response to nitrosative stress in *Saccharomyces cerevisiae*. *Mol. Biol. Cell*. 16:4781–4791. doi:10.1091/mbc.E05-05-0436
- Schuck, S., W.A. Prinz, K.S. Thorn, C. Voss, and P. Walter. 2009. Membrane expansion alleviates endoplasmic reticulum stress independently of the unfolded protein response. *J. Cell Biol.* 187:525–536. doi:10.1083/jcb.200907074
- Shamu, C.E., and P. Walter. 1996. Oligomerization and phosphorylation of the Ire1p kinase during intracellular signaling from the endoplasmic reticulum to the nucleus. *EMBO J.* 15:3028–3039.
- Sidrauski, C., and P. Walter. 1997. The transmembrane kinase Ire1p is a site-specific endonuclease that initiates mRNA splicing in the unfolded protein response. *Cell*. 90:1031–1039. doi:10.1016/S0092-8674(00)80369-4
- Travers, K.J., C.K. Patil, L. Wodicka, D.J. Lockhart, J.S. Weissman, and P. Walter. 2000. Functional and genomic analyses reveal an essential coordination between the unfolded protein response and ER-associated degradation. *Cell*. 101:249–258. doi:10.1016/S0092-8674(00)80835-1

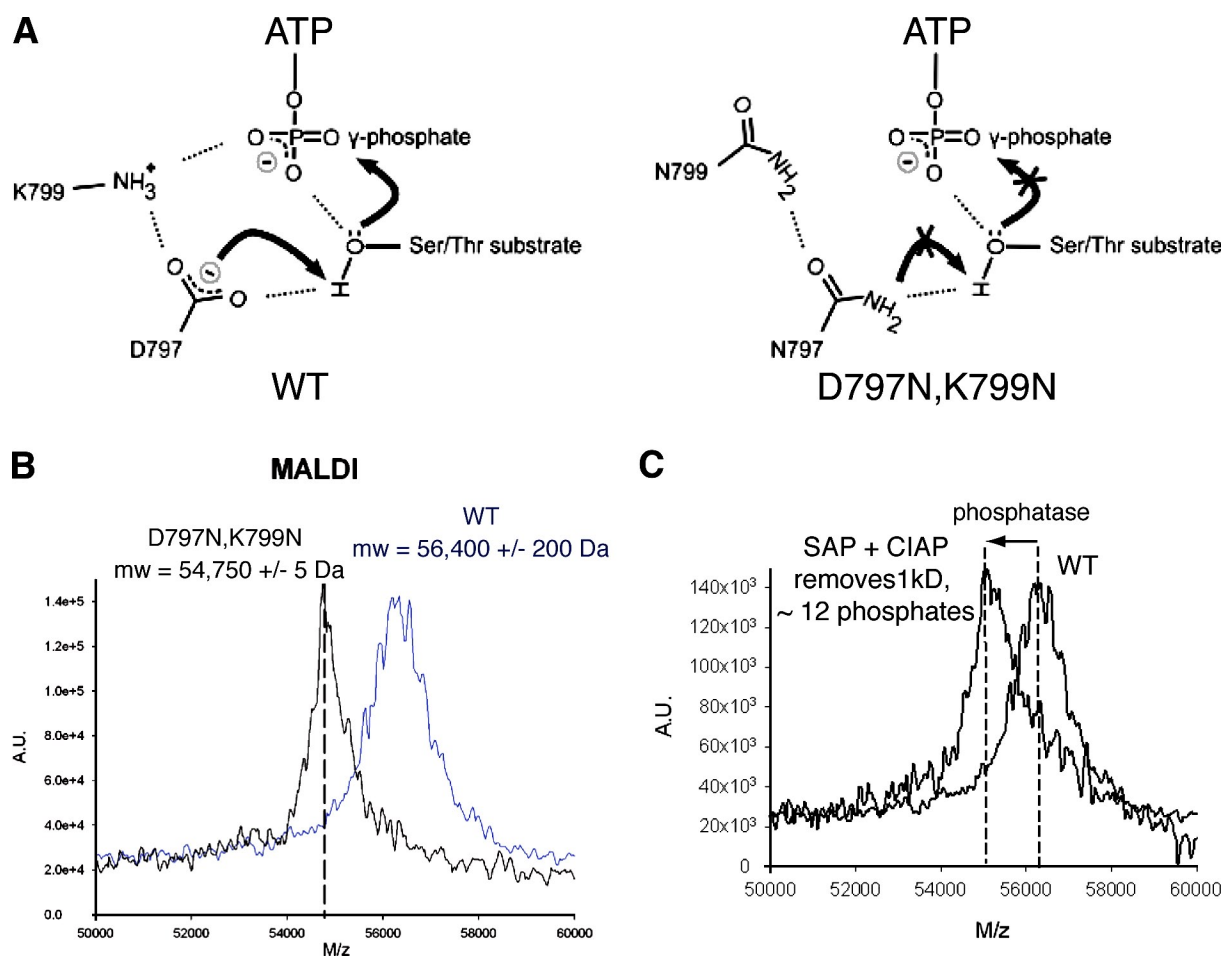
Rubio et al., <http://www.jcb.org/cgi/content/full/jcb.201007077/DC1>

Figure S1. **Mutations in Ire1 kinase abolish phosphoryl-transfer.** (A) Schematic diagram depicting predicted hydrogen bonding and proton transfer between key residues in the nucleotide-binding pocket of Ire1 kinase. (B) Recombinant Ire1(D797N,K799N) is unphosphorylated. MALDI mass spectrometry of purified recombinant Ire1KR32 reveals that the mass-to-charge ratio of WT Ire1KR32 (observed molecular weight ($m_{w,obs}$): $56,400 \pm 200$ D; calculated m_w : $54,767.22$ D) is ~ 1.3 kD higher than expected from its amino acid composition. A 1.3-kD shift in molecular weight corresponds to ~ 17 phosphates. The $m_{w,obs}$ of Ire1KR32(D797N,K799N) was $54,750 \pm 5$ D, consistent with the calculated m_w : $54,752.15$ D. (C) Phosphatase treatment of recombinant Ire1KR32 reduces its M/z value to its true molecular weight + 0.2 kD. This reduction in molecular weight is consistent with the removal of ~ 12 phosphates. Phosphatase-treated Ire1KR32 has a $m_{w,obs} = 55,050 \pm 50$ D and a calculated $m_w = 54,767.22$ D.

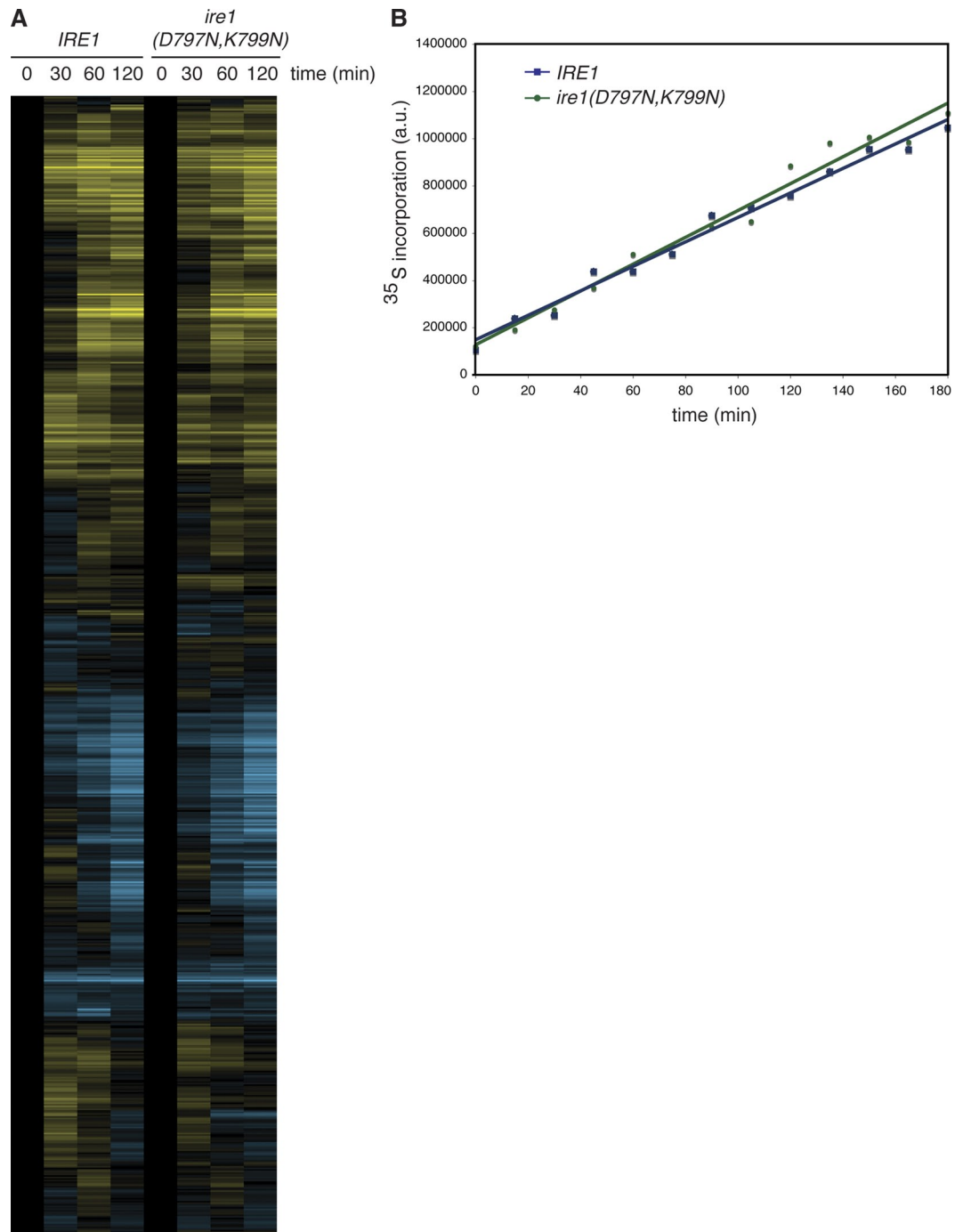


Figure S2. **The transcriptional response and global translation rates are normal in *ire1*(D797N,K799N) cells.** (A) Microarray analysis of genome-wide mRNA abundance. Total mRNA expression profiles of WT and *ire1*(D797N,K799N) cells were determined over a 2-h time course of UPR induction. (B) Global translation rates were measured by [³⁵S]-methionine incorporation over a 3-h time course of UPR induction. [³⁵S]-scintillation counts were normalized to cell number and plotted over time (P = 0.12).

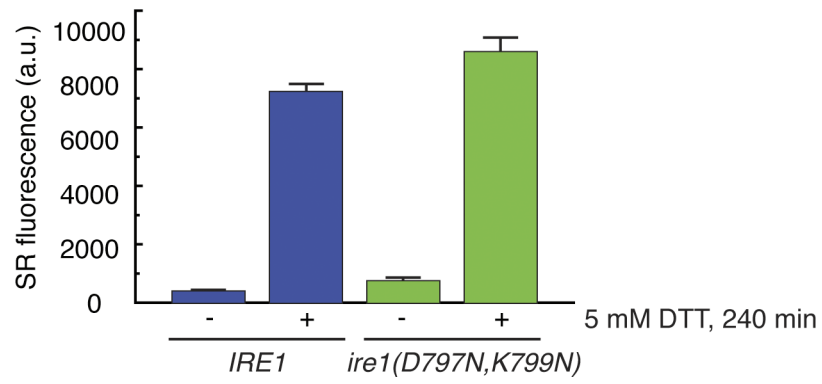


Figure S3. **The fold change of SR splicing in WT and *ire1(D797N,K799N)* cells is comparable.** Minimum (0% or -DTT) and maximum (100% or +DTT) values were taken from SR splicing assays using 5 mM DTT at times 0 and 240 min, respectively.